Mechanism of Basal-Plane Antiferromagnetism in the Spin-Orbit Driven Iridate Ba_2IrO_4

Vamshi M. Katukuri,[1] Viktor Yushankhai,[1,2] Liudmila Siurakshina,[2,3] Jeroen van den Brink,[1] Liviu Hozoi,[1] and Ioannis Rousochatzakis[1,3]

[1]*Institute for Theoretical Solid State Physics, IFW Dresden, Helmholtzstrasse 20, 01069 Dresden, Germany*

[2]*Joint Institute for Nuclear Research, Joliot-Curie 6, 141980 Dubna, Russia*

[3]*Max-Planck-Institut für Physik komplexer Systeme, Nöthnitzer Strasse 38, 01187 Dresden, Germany*

(Received 13 February 2014; revised manuscript received 18 April 2014; published 17 June 2014)

By *ab initio* many-body quantum chemistry calculations, we determine the strength of the symmetric anisotropy in the $5d^5$ $j \approx 1/2$ layered material Ba_2IrO_4. While the calculated anisotropic couplings come out in the range of a few meV, orders of magnitude stronger than in analogous $3d$ transition-metal compounds, the Heisenberg superexchange still defines the largest energy scale. The *ab initio* results reveal that individual layers of Ba_2IrO_4 provide a close realization of the quantum spin-1/2 Heisenberg-compass model on the square lattice. We show that the experimentally observed basal-plane antiferromagnetism can be accounted for by including additional interlayer interactions and the associated order-by-disorder quantum-mechanical effects, in analogy to undoped layered cuprates.

DOI: 10.1103/PhysRevX.4.021051

Subject Areas: Condensed Matter Physics, Magnetism, Strongly Correlated Materials

I. INTRODUCTION

The few varieties of square-lattice effective spin models are emblematic in modern quantum magnetism and extensively investigated in relation to layered superconducting materials such as the copper oxides [1] and iron pnictides or chalcogenides [2]. While the dominant magnetic energy scale is set in these systems by the isotropic Heisenberg exchange between nearest-neighbor (NN) [3] and possibly next-NN sites [4], there are many examples where the smaller, anisotropic terms become important too, e.g., for correctly describing the antiferromagnetic (AFM) ordering pattern in La_2CuO_4 [5] or in the cuprate oxychlorides [6,7]. This topic, the role of anisotropic interactions in transition-metal compounds, has received a new impetus with recent insights into the basic electronic structure of $5d$ systems such as the $5d^5$ iridium oxides. Here, a subtle interplay between spin-orbit interactions and sizable electron correlations gives rise to insulating ground states and well-protected magnetic moments [8–13]. Because of the strong spin-orbit couplings, however, these magnetic moments are best described as effective $j \approx 1/2$ entities [9,10,14] and the effective anisotropic exchange parameters are orders of magnitude larger than in $3d$ transition-metal compounds. For the square-lattice system Sr_2IrO_4, for instance, Dzyaloshinskii-Moriya (DM) interactions as large as one quarter of the NN AFM superexchange have been predicted [15,16] while in honeycomb iridates the symmetric Kitaev exchange is believed to be even larger than the Heisenberg interaction [17–20].

Valuable insights into the role of different superexchange processes in correlated d-metal oxides come from the detailed analysis of extended multiorbital Hubbard-type models. The foundations of superexchange theory were laid as early as the 1950s with the work of Anderson, Goodenough, and Kanamori [21]. Standard approaches within this theoretical framework proved to be extremely useful in, e.g., better understanding the origin and relative strength of the anisotropic couplings in layered cuprates [22,23]. In 2D iridates, on the other hand, much less information is presently available on the magnitude of various electronic-structure parameters that enter the superexchange models. While estimates for these effective electronic-structure parameters are normally based on either density-functional band-structure calculations [15,16,18,24,25] or experiments [10,11,13,17,20], here we rely on many-body quantum-chemistry methods to directly obtain an *ab initio* assessment of both the NN Heisenberg exchange and the anisotropic couplings on the square lattice of Ba_2IrO_4. Our study reveals uniaxial symmetric anisotropy that is bond dependent, thus giving rise to quantum compass interaction terms [26] superimposed onto the much stronger (due to the 180° bond geometry) isotropic Heisenberg exchange. We also show that the resulting Heisenberg-compass model for individual layers of Ba_2IrO_4 is not sufficient to explain the AFM ground-state ordering pattern inferred from recent resonant magnetic scattering measurements, with spins ordered along the [110] direction [12]. To rationalize the latter,

we carry out a detailed analysis of the role of interlayer couplings and the associated order-by-disorder phenomena. An extended 3D spin Hamiltonian based on NN exchange terms as found in the *ab initio* quantum-chemistry calculations and additional farther-neighbor interlayer exchange integrals turns out to provide a realistic starting point to explain the magnetism of Ba_2IrO_4.

II. GENERAL CONSIDERATIONS

The magnetically active sites, the Ir^{4+} ions, have a $5d^5$ valence electron configuration in Ba_2IrO_4, which under strong octahedral crystal-field and spin-orbit interactions yields an effective $j \approx 1/2$ Kramers-doublet ground state; see Refs. [10,12,14,27]. The exchange interactions between such pseudospin entities involve both isotropic Heisenberg and anisotropic terms. For a pair of NN pseudospins $\tilde{\mathbf{S}}_i$ and $\tilde{\mathbf{S}}_j$, the most general bilinear spin Hamiltonian can be cast in the form

$$\mathcal{H}_{ij} = J_{ij}\tilde{\mathbf{S}}_i \cdot \tilde{\mathbf{S}}_j + \mathbf{D}_{ij} \cdot \tilde{\mathbf{S}}_i \times \tilde{\mathbf{S}}_j + \tilde{\mathbf{S}}_i \cdot \mathbf{\Gamma}_{ij} \cdot \tilde{\mathbf{S}}_j, \quad (1)$$

where J_{ij} is the isotropic Heisenberg exchange, the vector $\mathbf{D}_{ij}$ defines the DM anisotropy, and Γ_{ij} is a symmetric traceless second-rank tensor that describes the symmetric portion of the exchange anisotropy. Depending on various geometrical details and the choice of the reference frame, some elements of the DM vector and/or of the $\Gamma_{ij}^{\alpha\beta}$ tensor may be zero. For the square lattice of corner-sharing IrO_6 octahedra in Ba_2IrO_4, the symmetry of each block of two NN octahedra is D_{2h}, with inversion symmetry at the bridging oxygen site [28]. Given the inversion center, the DM anisotropy vanishes. The remaining symmetries require that, in the $\{xyz\}$ frame, with x along the Ir-Ir link and z orthogonal to the IrO_2 layers, Γ_{ij} is diagonal. The two-site effective spin Hamiltonian for an Ir-Ir link along the x axis can then be written as

$$\mathcal{H}_{\langle ij\rangle \| x} = J\tilde{\mathbf{S}}_i \cdot \tilde{\mathbf{S}}_j + \Gamma_{\|}\tilde{S}_i^x\tilde{S}_j^x + \Gamma_{\perp}\tilde{S}_i^y\tilde{S}_j^y + \Gamma_{zz}\tilde{S}_i^z\tilde{S}_j^z, \quad (2)$$

with $\Gamma_{zz} = -(\Gamma_{\|} + \Gamma_{\perp})$ since $\mathbf{\Gamma}$ is traceless. Because of the fourfold z-axis symmetry, we analogously have

$$\mathcal{H}_{\langle ij\rangle \| y} = J\tilde{\mathbf{S}}_i \cdot \tilde{\mathbf{S}}_j + \Gamma_{\|}\tilde{S}_i^y\tilde{S}_j^y + \Gamma_{\perp}\tilde{S}_i^x\tilde{S}_j^x + \Gamma_{zz}\tilde{S}_i^z\tilde{S}_j^z \quad (3)$$

for bonds along the y axis. The eigenstates of Eq. (2) are the singlet $|\Psi_S\rangle = (|\uparrow\downarrow\rangle - |\downarrow\uparrow\rangle)/\sqrt{2}$ and the three "triplet" components $|\Psi_1\rangle = (|\uparrow\downarrow\rangle + |\downarrow\uparrow\rangle/\sqrt{2})$, $|\Psi_2\rangle = (|\uparrow\uparrow\rangle + |\downarrow\downarrow\rangle/\sqrt{2})$, $|\Psi_3\rangle = (|\uparrow\uparrow\rangle - |\downarrow\downarrow\rangle/\sqrt{2})$. The corresponding eigenvalues are

$$E_S = -\frac{3}{4}J, \qquad E_1 = \frac{1}{4}J + \frac{1}{2}(\Gamma_{\|} + \Gamma_{\perp}),$$
$$E_2 = \frac{1}{4}J - \frac{1}{2}\Gamma_{\perp}, \qquad E_3 = \frac{1}{4}J - \frac{1}{2}\Gamma_{\|}. \quad (4)$$

For D_{2h} symmetry of the two-octahedra unit, the four low-lying (spin-orbit) states, $|\Psi_S\rangle$, $|\Psi_1\rangle$, $|\Psi_2\rangle$, and $|\Psi_3\rangle$, transform according to the A_{1g}, B_{2u}, B_{1u}, and A_{1u} irreducible representations, respectively [19]. As we discuss in the following, this symmetry analysis is useful in determining the nature of each of the low-lying many-body states in the quantum-chemistry calculations.

III. QUANTUM-CHEMISTRY CALCULATIONS

A. Computational details

The crystalline unit cell of Ba_2IrO_4 is sketched in Fig. 1(a). NN in-plane exchange paths are indicated for the upper IrO_2 layer. The relevant NN effective coupling constants, i.e., the isotropic Heisenberg J and the components of the symmetric anisotropic exchange Γ, are defined in Eqs. (2) and (3). Both J and the set of Γ's are determined here at various levels of approximation by *ab initio* quantum-chemistry methods. Interlayer exchange paths are also shown in Fig. 1(a). These out-of-plane couplings are characterized by an isotropic exchange J_{out} plus the symmetric second-rank tensor Γ_{out} for the symmetric anisotropy and included at a later stage in our analysis to explain the 3D magnetic structure of Ba_2IrO_4.

The NN in-plane magnetic coupling constants are obtained on the basis of multireference configuration-interaction (MRCI) calculations [29] on units of two corner-sharing IrO_6 octahedra. Since it is important to accurately describe the charge distribution at sites in the immediate neighborhood [30–32], we also include in the actual cluster the closest 16 Ba ions and the six adjacent IrO_6 octahedra around the reference $[Ir_2O_{11}]$ fragment; see Fig. 1 and also Refs. [19,33–35]. However, to make the whole analysis tractable, we replace the six Ir^{4+} d^5 NNs by closed-shell Pt^{4+} d^6 ions, a usual procedure in

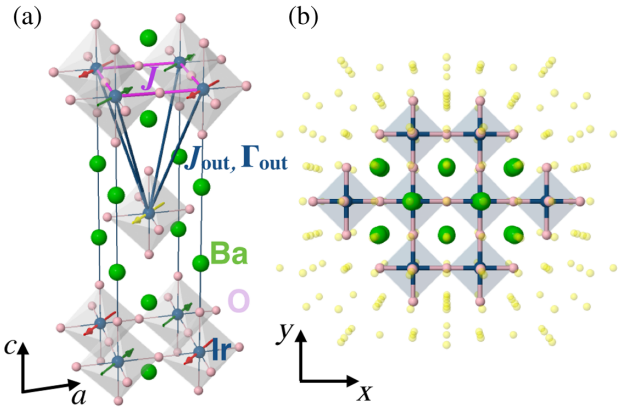

FIG. 1. (a) Layered crystal structure of Ba_2IrO_4. In-plane and interlayer exchange paths are shown. (b) Sketch of the cluster used for the calculation of the in-plane NN magnetic interactions. It consists of a central $[Ir_2O_{11}]$ fragment of two corner-sharing IrO_6 octahedra and six other adjacent octahedra; see text. Ir, O, and Ba ions are shown in blue, pink, and green, respectively.

quantum-chemistry investigations on d-metal systems [19,33–37]. The extended solid-state surroundings are modeled as a large array of point charges fitted to reproduce the crystal Madelung field in the cluster region. We use the crystal structure reported by Okabe *et al.* [28].

All calculations are performed with the MOLPRO quantum-chemistry software [38]. Energy-consistent relativistic pseudopotentials from the standard MOLPRO library are used for Ir [39] and Ba [40]. The valence orbitals at the central Ir sites are described by basis sets of quadruple-zeta quality supplemented with two f polarization functions [39], while we apply quintuple-zeta valence basis sets and four d polarization functions for the ligand bridging the two magnetically active Ir ions [41]. The other O's at the two central octahedra are modeled by triple-zeta valence basis sets [41]. For the additional ligands coordinating the six adjacent $5d$ sites, we use minimal atomic-natural-orbital basis functions [42]. At those adjacent $5d$ sites, we apply triple-zeta valence basis sets [39].

Multiconfiguration reference wave functions were first generated by complete-active-space self-consistent-field (CASSCF) calculations [29]. The active space here is given by five electrons and three (t_{2g}) orbitals at each of the two magnetically active Ir sites. The orbitals are optimized for an average of the lowest nine singlet and the nine triplet states arising from such an active space. All of these states enter the spin-orbit calculations, at both the CASSCF and MRCI levels. In the MRCI treatment, single and double excitations from the six Ir t_{2g} orbitals and the $2p$ shell of the bridging ligand site are taken into account. Similar strategies of explicitly dealing with only selected groups of localized ligand orbitals were adopted in earlier studies on both $3d$ [43–46] and $5d$ [19,33–35] compounds, with results in good agreement with the experiment [33,34,44–46]. To separate the metal $5d$ and O $2p$ valence orbitals into different groups, we use the orbital localization module available in MOLPRO. The MRCI is performed for each spin multiplicity, singlet or triplet, as a nine-root calculation.

To obtain information on the magnitude of the direct exchange, we additionally carry out single-configuration restricted open-shell Hartree-Fock (ROHF) calculations [29]. The latter are performed as frozen-orbital calculations, i.e., we use the orbitals obtained by CASSCF (see above), without further optimization.

The spin-orbit treatment is carried out according to the procedure described in Ref. [47]. To determine the nature of each spin-orbit state, we explicitly compute with MOLPRO the dipole and quadrupole transition matrix elements among those four low-lying states describing the magnetic spectrum of two corner-sharing octahedra; see Table I and Sec. III B. Standard selection rules and the nonzero dipole and quadrupole matrix elements in the quantum-chemistry outputs then clearly indicate which state is which; see also the analysis and discussion in Ref. [19].

TABLE I. Energy splittings for the four lowest spin-orbit states of two NN IrO_6 octahedra and the corresponding effective coupling constants in Ba214, at different levels of approximation (all in meV).

States	HF + SOC	CAS + SOC	CI + SOC
$\Psi_S(A_{1g}) = (\uparrow\downarrow - \downarrow\uparrow)/\sqrt{2}$	12.2	0.0	0.0
$\Psi_3(A_{1u}) = (\uparrow\uparrow - \downarrow\downarrow)/\sqrt{2}$	0.0	37.5	65.0
$\Psi_1(B_{2u}) = (\uparrow\downarrow + \downarrow\uparrow)/\sqrt{2}$	0.2	38.2	66.7
$\Psi_2(B_{1u}) = (\uparrow\uparrow + \downarrow\downarrow)/\sqrt{2}$	0.2	38.2	66.7
$(\bar{J}, \bar{\Gamma}_\parallel)$	(−12.0,0.4)	(37.5,1.4)	(65.0,3.4)

B. *Ab initio* results

Of the 36 spin-orbit states that are obtained in the *ab initio* calculations, the low-lying four are listed in Table I [48]. These four states are further mapped onto the eigenvalues of the effective spin Hamiltonian in Eq. (2). Energy splittings and the associated effective magnetic couplings are provided at three levels of approximation: single-configuration ROHF (HF + SOC), CASSCF (CAS + SOC), and MRCI (CI + SOC). It is seen that, at all levels of theory, two of the triplet components, Ψ_1 and Ψ_2, are degenerate [49]. Given the tetragonal distortions in Ba_2IrO_4, with out-of-plane (z axis) Ir-O bonds significantly stretched as compared to the in-plane (x/y) bonds [28], this degeneracy is somewhat surprising. Using Eq. (4), this means that two of the diagonal couplings of Γ are equal, $\Gamma_{zz} = \Gamma_\perp$, which further implies $\Gamma_\parallel = -2\Gamma_\perp$. The interaction terms in Eqs. (2) and (3) can then be rewritten as

$$\mathcal{H}_{\langle ij\rangle\parallel x} = \bar{J}\tilde{\mathbf{S}}_i \cdot \tilde{\mathbf{S}}_j + \bar{\Gamma}_\parallel \tilde{S}_i^x \tilde{S}_j^x,$$
$$\mathcal{H}_{\langle ij\rangle\parallel y} = \bar{J}\tilde{\mathbf{S}}_i \cdot \tilde{\mathbf{S}}_j + \bar{\Gamma}_\parallel \tilde{S}_i^y \tilde{S}_j^y, \quad (5)$$

where $\bar{J} \equiv J + \Gamma_\perp$ and $\bar{\Gamma}_\parallel \equiv -3\Gamma_\perp$. Quantum-chemistry results for $\bar{J}$ and $\bar{\Gamma}_\parallel$ are provided on the lowest line in Table I.

The value computed for the Heisenberg $\bar{J}$ within the ROHF approximation, −12 meV (see Table I), is sizable and close to the results computed in square-lattice $3d^9$ Cu oxides (see, e.g., Ref. [44]). It accounts for only direct exchange, since no (intersite) excitations are allowed. In contrast to the ROHF $\bar{J}$, the anisotropic $\bar{\Gamma}_\parallel$ is AFM by ROHF.

With correlated wave functions, CASSCF and MRCI, the singlet Ψ_S becomes the ground state, well below the triplet components Ψ_1, Ψ_2, and Ψ_3. This shows that the largest energy scale is defined here by the isotropic Heisenberg exchange $\bar{J}$ ($\bar{J} > 0$). In the CASSCF approximation, only intersite d-d excitations as analyzed by Anderson [21] are accounted for, i.e., polar t_{2g}^6–t_{2g}^4 configurations. Again, the CAS + SOC $\bar{J}$, 37.5 meV, is very similar to the CASSCF J's in layered $3d^9$ cuprates [44,50,51]. It is seen in Table I that the configuration-interaction treatment, which now includes $t_{2g}^5 e_g^1$–t_{2g}^4 and O

$2p$ to Ir $5d$ charge-transfer virtual states as well, enhances $\bar{J}$ by about 70% as compared to the CAS + SOC value, somewhat less spectacular than the ratio between the configuration interaction and CASSCF J's in layered cuprates. In the latter compounds, this ratio is 3:4 [44,52].

If we include in the MRCI treatment only the six Ir t_{2g} orbitals, $\bar{J}$ is 49.1 meV (not shown in Table I). The difference between the latter number and the CAS + SOC value given in Table I is indicative of the role of excitation processes via the Ir $5d$ e_g levels. The further increase from 49.1 to 65 meV is due to excitations that additionally involve the bridging O $2p$ orbitals. The data in Table I also show that the correlation treatment very much enlarges the symmetric anisotropic coupling $\bar{\Gamma}_{\|}$, from 0.4 by ROHF to 3.4 meV by MRCI.

IV. COMPARISON TO EFFECTIVE SUPEREXCHANGE MODELS

For the Mott-like insulating regime occurring in the iridates [8–10], an effective superexchange model can be in a first approximation set up by considering the leading excited configurations with two holes at the same Ir site. With corner-sharing octahedra and straight Ir-O-Ir bonds along the x axis, the intersite d-d hopping takes place via both in-plane p_y and out-of-plane p_z π-type O orbitals. The relevant effective hopping integrals are $t_1 = (t_{pd}^{\pi})^2/|\epsilon_d^{xy} - \epsilon_p^{y}|$ for the in-plane, xy pair of NN Ir t_{2g} functions, and $t_2 = (t_{pd}^{\pi})^2/|\epsilon_d^{xz} - \epsilon_p^{z}|$ for the out-of-plane, xz t_{2g} functions. $\epsilon_p^{y/z}$ and $\epsilon_d^{xy/xz} = \epsilon_{1/2}$ here are crystal-field split energy levels while the p-d π-type hopping amplitude t_{pd}^{π} is assumed to be the same for both channels.

For tetragonal distortions, $\epsilon_1 \neq \epsilon_2$, $\epsilon_p^{y} \neq \epsilon_p^{z}$ and, therefore, t_1 and t_2 may acquire quite different values. A hole hopping between NN Ir ions is then described by the Hamiltonian

$$H_{\mathrm{hop}}^{ij} = \sum_{m=1,2} \sum_{\sigma=\uparrow,\downarrow} (t_m d_{im\sigma}^{\dagger} d_{jm\sigma} + \mathrm{H.c.}), \qquad (6)$$

where $d_{im\sigma}^{\dagger}(d_{im\sigma})$ is the creation (annihilation) operator of a hole with spin σ in the orbital d_{xy} for $m = 1$ and d_{xz} for $m = 2$ at site i. For a bond along the y axis, p_y is replaced by p_x, d_{xz} by d_{yz}, $\epsilon_p^{y} = \epsilon_p^{x}$, $\epsilon_3 = \epsilon_d^{yz} = \epsilon_d^{xz} = \epsilon_2$, and the hopping Hamiltonian in Eq. (6) has the same form.

The interaction of two holes in the t_{2g} subshell is described by Hund's coupling J_H and the Coulomb repulsion integrals $U_{mm'} \simeq U - 2J_H$, if $m \neq m'$, and $U_{mm} = U$. While the isotropic exchange is related to second-order processes that concern transitions between the lowest spin-orbit Kramers doublets, i.e., $J \sim t_{1/2}^2/U$, the symmetric anisotropy is entirely determined by third-order processes that involve excited Kramers doublets, i.e., is dependent on $t_{1/2}^2 J_H/U^2$.

The lowest Kramers-doublet wave functions

$$|\tilde{\uparrow}\rangle = \sin\theta|xy,\uparrow\rangle + \frac{\cos\theta}{\sqrt{2}}(i|xz,\downarrow\rangle + |yz,\downarrow\rangle),$$
$$|\tilde{\downarrow}\rangle = \sin\theta|xy,\downarrow\rangle - \frac{\cos\theta}{\sqrt{2}}(i|xz,\uparrow\rangle - |yz,\uparrow\rangle), \qquad (7)$$

as well as those for the excited Kramers doublets, are parametrized here as in Ref. [10], with the angle θ given by $\tan(2\theta) = 2\sqrt{2}\lambda/(\lambda - 2\Delta)$ while $\Delta = \epsilon_2^d - \epsilon_1^d$ is the tetragonal t_{2g} splitting.

By collecting the second- and third-order processes in this effective superexchange model, we arrive at the pseudospin Hamiltonian in Eq. (2), with

$$J = \frac{4}{U}\left(t_1\sin^2\theta + \frac{t_2}{2}\cos^2\theta\right)^2 + \gamma,$$
$$\Gamma_{\|} = -\eta\frac{3(t_1 - t_2)^2}{U}\sin^2\theta\cos^2\theta - \gamma,$$
$$\Gamma_{\perp} = -\eta\frac{3t_1^2}{U}\sin^2\theta\cos^2\theta - \gamma,$$
$$\Gamma_{zz} = -\eta\frac{3t_2^2}{2U}\cos^4\theta - \gamma. \qquad (8)$$

Here, $\eta = J_H/U$ and $\gamma = -(\eta/U)\cos^2\theta[(t_1 - t_2)^2\sin^2\theta + t_1^2\sin^2\theta + \frac{1}{2}t_2^2\cos^2\theta]$.

Now, for $\Gamma_{zz} = \Gamma_{\perp}$, the model described by Eq. (5) displays uniaxial compasslike anisotropy [26]. That is obviously the case for perfect, cubic octahedra with $\Delta = 0$, $t_1 = t_2 = t$, and $\cos\theta_c = \sqrt{2}\sin\theta_c = \sqrt{2/3}$. In the cubic limit, from Eq. (8) we further have $J^c = (16/9)t^2/U + \gamma^c$, $\gamma^c = -(4\eta/9)t^2/U$, $\Gamma_{\|}^c = -\gamma^c$, and $\Gamma_{\perp}^c = \Gamma_{zz}^c = (-2\eta/3)t^2/U - \gamma^c$.

For tetragonal distortions as found in Ba_2IrO_4 [28], $\Gamma_{\perp} = \Gamma_{zz}$ implies that $(t_2/t_1)^2 = 2\tan^2\theta$. As a measure of how large the departure from the cubic limit is, we can take the ratio between the tetragonal t_{2g} splitting Δ and the strength of the spin-orbit coupling λ. The quantum-chemistry calculations yield $\Delta = 65$ meV in Ba_2IrO_4 (see the discussion in Ref. [53]), in agreement with estimates based on experiment [27]. A direct estimate of the spin-orbit coupling can also be obtained, from the splitting of the $j = 1/2$ and $j = 3/2$ t_{2g}^5 states for idealized cubic octahedra. It turns out that for perfect octahedra $\lambda = 0.47$ eV [34,53], close to values of 0.4–0.5 eV previously derived from electron spin resonance and optical measurements on $5d^5$ ions [54–57]. The ratio Δ/λ is, therefore, rather small, ≈ 0.15.

Estimates for the parameters that enter the effective superexchange model can most easily be obtained in the cubic limit. Using Eq. (8), we find that $\bar{\Gamma}_{\|}/\bar{J} \approx (3/8)\eta$. The CI + SOC values of Table I, $\bar{\Gamma}_{\|} = 3.4$ and $\bar{J} = 65$ meV, then lead to $\eta \approx 0.14$ and $4t^2/U \approx 149$ meV. Interestingly, estimates of the hopping integral t from calculations based

on density-functional theory (DFT) are $t_{\rm DFT} \approx 260$ meV, while the on-site Coulomb repulsion comes out from constrained calculations in the random phase approximation (RPA) as $U_{\rm RPA} \approx 1.65$ eV [25]. The ratio $4t_{\rm DFT}^2/U_{\rm RPA}$ is, therefore, ≈164 meV, close to the result derived on the basis of the CI+SOC effective couplings listed in Table I. On the other hand, the η parameter extracted from the periodic DFT calculations [25] is $\eta_{\rm DFT} \approx 0.08$, much smaller than the above value of 0.14. Using the latter value for η, $\eta_{\rm DFT} \approx 0.08$, an estimate for the symmetric anisotropic coupling $\bar{\Gamma}_{\parallel} = (3/8)\eta\bar{J}$ would be significantly smaller than the quantum-chemistry result.

V. GROUND-STATE PHASE DIAGRAM

Having established the strength of the dominant in-plane exchange interactions and anisotropies, we now turn to the nature of the magnetic ground state of Ba_2IrO_4, focusing first on a single square-lattice IrO_2 layer. In the classical limit, the compass-Heisenberg model defined by Eq. (5) has an accidental SO(2) ground-state degeneracy, with spins pointing along any direction in the basal xy plane [26,58,59]. This degeneracy is eventually lifted via thermal [60–62] or quantum [23,62–64] order-by-disorder effects, whereby harmonic spin wave fluctuations select the states with spins pointing either along the x or y axis. This is, however, in sharp contrast to experiments that below ∼240 K show basal-plane AFM order with magnetic moments along the [110] direction [12]. It indicates additional anisotropies in the system, large enough to overcome the energy gain from the order-by-disorder mechanism.

The situation is actually analogous to several $3d^9$ Cu oxides with the same "214" crystal structure as Ba_2IrO_4. It has been shown that in cuprates that particular type of AFM order is selected by a subtle interplay between in-plane and interlayer interactions, as discussed in detail in Ref. [23]. Assuming that qualitatively the same 3D mechanism is applicable to Ba_2IrO_4, below we analyze the main contributions to the expression of the 3D ground-state energy and derive a generic phase diagram. This exercise provides useful insights into the dependence of the ground-state spin configuration on various interaction parameters in 214 iridates.

It turns out that the most important effects competing with the in-plane NN interactions concern (i) the frustrating nature of the isotropic interlayer exchange and (ii) the symmetric part of the anisotropic exchange between layers. To show this, we proceed by parametrizing the global spin direction in each basal plane by an angle ϕ_n, where n is the layer index, and by writing down all relevant energy contributions.

The first contribution is the zero-point energy (per spin) coming from the order-by-disorder mechanism in each individual layer, $E_{\rm ZP,2D}(\{\phi_n\}) = \sum_n \mathcal{E}_{\rm ZP,2D}(\phi_n)$, where

$$\mathcal{E}_{\rm ZP,2D}(\phi) = \frac{1}{2N}\sum_{\mathbf{q}}[\omega_+(\mathbf{q}) + \omega_-(\mathbf{q})], \tag{9}$$

and $\omega_\pm(\mathbf{q})$ are the two spin wave branches. Summation over the Brillouine zone is implied in Eq. (9) and the explicit dependence of $\omega_\pm(\mathbf{q})$ on ϕ is provided by expressions in Appendix A. A numerical analysis of Eq. (9), using the *ab initio* quantum-chemistry values for the in-plane NN effective couplings (see Sec. III), shows that $\mathcal{E}_{\rm ZP,2D}(\phi)$ is almost identical to the expression

$$\mathcal{E}_{\rm ZP,2D}(\phi) = -K\cos(4\phi) + E_0, \tag{10}$$

with $K = 0.86$ μeV and $E_0 = 56.55$ meV.

We now turn to the second contribution to the energy, which stems from the interlayer isotropic exchange $J_{\rm out}$. Despite being the dominant portion of the interlayer interactions, its total contribution to the energy vanishes in the mean-field sense due to geometric frustration in the 214 structure; see Fig. 1. Yet, quantum fluctuations driven by $J_{\rm out}$ still give rise to a zero-point energy contribution [22,23]

$$E_{\rm ZP,3D}(\{\phi_n\}) = -B\sum_n \cos(2\phi_n - 2\phi_{n+1}), \tag{11}$$

where $B \simeq 0.032J_{\rm out}^2/(2J_{\rm av})$ and $J_{\rm av} = J + (\Gamma_\parallel + \Gamma_\perp)/2$ [see Eq. (53) in Ref. [23] and references therein]. Since B is positive for any sign of $J_{\rm out}$, this contribution favors collinearity of the staggered magnetization in adjacent layers.

The third contribution to the energy comes from the anisotropic portion of the interlayer couplings. We first note that the antisymmetric DM component vanishes by symmetry since the midpoint of each out-of-plane NN Ir-Ir link is an inversion center. The remaining, symmetric portion can be described by a traceless second-rank tensor $\Gamma_{\rm out}$. The structure of the latter is simplified by using the fact that each of the out-of-plane NN Ir-Ir links has C_{2h} symmetry, with the $\{110\}$ plane as a mirror plane (see Fig. 1). The principal values of $\mathbf{\Gamma}_{\rm out}$ are denoted as $\Gamma_{\rm out}^{\perp}$, $\Gamma_{\rm out}^{\parallel,1}$, and $\Gamma_{\rm out}^{\parallel,2}$, where $\Gamma_{\rm out}^{\perp}$ is for the principal axis perpendicular to the mirror plane and the other two elements correspond to two mutually orthogonal axes within the $\{110\}$ plane. The orientation of the in-plane principal axes with respect to the tetragonal z axis is given by some angle β [23]. Having the tensor $\Gamma_{\rm out}$ for one Ir-Ir link, the corresponding coupling terms for the other three out-of-plane NN Ir-Ir links emerging out of a given Ir site are determined by symmetry. Adding up these symmetric anisotropic contributions for all four NN bonds above and below the square-lattice layer at a reference Ir site yields [23]

$$E_{\mathrm{aniso,3D}} = -A\sum_n \sin(\phi_n + \phi_{n+1}), \tag{12}$$

where $A = (1/4)(\Gamma^{\parallel,1}_{\mathrm{out}} - \Gamma^{\perp}_{\mathrm{out}})\cos\beta$.

The total energy now reads

$$E = E_{\mathrm{ZP,2D}} + E_{\mathrm{ZP,3D}} + E_{\mathrm{aniso,3D}}. \tag{13}$$

It can be minimized analytically as described in Appendix B by working it out for a bilayer of Ba214. The resulting phase diagram in the $(A/K, B/K)$ plane is shown in Fig. 2 for positive A (the phase diagram for $A < 0$ is identical, see Appendix B) and hosts three different phases, two collinear (phases I and II) and one noncollinear (phase III).

In phase I, the staggered magnetizations point along one of the $\langle 110\rangle$ axes and the relative directions between adjacent planes are regularly collinear or anticollinear. In phase III, the AFM magnetization prefers one of the $\langle 100\rangle$ axes and the relative directions in adjacent planes are now perpendicular to each other. Finally, in phase II, the relative directions between adjacent planes are again either collinear or anticollinear, but the staggered magnetizations in each layer rotate in the basal plane as a function of A/K; see Appendix B. Importantly, the degeneracy is not completely lifted by the above couplings. As explained in Appendix B, all phases have an Ising degree of freedom per layer, which comes from the fact that the energy remains the same if we flip all spins within a given layer. This remaining macroscopic degeneracy may eventually be lifted via higher-order processes or farther-neighbor couplings; see, for example, the discussion in Ref. [22]. The collinear AFM structure observed experimentally [12] in Ba_2IrO_4 can now be naturally explained provided that A and B fall into the broad region of phase I in the phase diagram of Fig. 2 and by taking into account lifting of the remaining Ising degeneracy by the mechanism mentioned above.

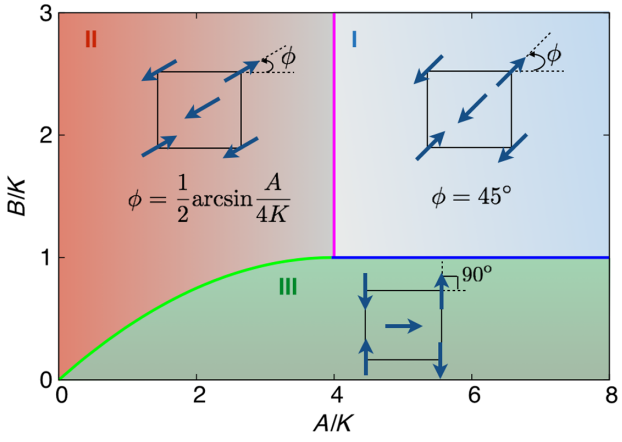

FIG. 2. Ground-state phase diagram of the model described in Sec. V, including the single-layer Heisenberg-compass terms of Eq. (5) plus the effect of interlayer (isotropic and anisotropic) exchange. The in-plane coupling constants are taken as obtained in the *ab initio* CI + SOC calculations, while the effective interactions A, B, and K are defined through Eqs. (10)–(12); see text.

As pointed out by Boseggia *et al.* [12], the AFM component of the ordered momenta in the 214 iridates Sr_2IrO_4 and Ba_2IrO_4 is essentially identical: in Sr_2IrO_4, the canted AFM state is characterized by an AFM vector aligned along the $\langle 110\rangle$ direction and a residual FM moment confined to the same basal plane. Staggered rotation of the IrO_6 octahedra as realized in Sr_2IrO_4 requires the more general single-layer Hamiltonian of Eq. (1) [10,16], with a DM vector along the z axis and a biaxial easy-plane symmetric anisotropy described in our notation by two independent diagonal components $\Gamma_{\parallel} > 0$ and $\Gamma_{zz} > 0$. This model correctly explains the canting angle of the basal-plane AFM order [16] but fails in predicting the AFM vector alignment along one of the $\langle 110\rangle$ axes. The reason is that the two additional anisotropies, $\mathbf{D}||z$ and $\Gamma_{zz} > 0$, do not remove the SO(2) basal-plane ground-state degeneracy, at least not in the classical limit. This accidental degeneracy can, however, again be lifted via the 3D mechanism discussed above, to arrive at an AFM ordering pattern similar to that of Ba_2IrO_4 [12].

VI. CONCLUSIONS

While *ab initio* quantum-chemistry techniques have previously been used to derive the sign and strength of the symmetric anisotropic (Kitaev) interactions in $5d^5$ iridates with edge-sharing IrO_6 octahedra [19], here we employ the same methodology to clarify the signs and magnitude of the symmetric anisotropic couplings for corner-sharing octahedra in the square-lattice compound Ba_2IrO_4. The *ab initio* results reveal effective uniaxial anisotropy, although the actual symmetry of each of the in-plane Ir-Ir links is lower than D_{4h}. The anisotropic effective coupling constants are as large as 3.5 meV, comparable in strength to the anisotropic Kitaev exchange in honeycomb Na_2IrO_3 [19]. However, in contrast to Na_2IrO_3, the largest energy scale is defined here by the Heisenberg J, with $J \approx 65$ meV. The latter value agrees with estimates based on resonant inelastic x-ray scattering measurements on 214 iridates [11]. Given the uniaxial structure of the exchange coupling tensor, the relevant in-plane (pseudo)spin model is a Heisenberg-compass type of model. Yet, to understand the experimentally determined AFM ordering pattern, with spins along the [110] direction [12], interlayer interactions must be included in the effective Hamiltonian. Further investigations are now being carried out in our group for quantifying the strength of Dzyaloshinskii-Moriya couplings for the closely related 214 compound Sr_2IrO_4, displaying bent Ir-O-Ir links. Another interesting issue is the dependence of the in-plane anisotropic couplings, their signs, in particular, on pressure [65] and strain [66], in both Ba_2IrO_4 and Sr_2IrO_4.

ACKNOWLEDGMENTS

We thank N. Perkins for useful discussions. L. H. acknowledges financial support from the German Research Foundation (Deutsche Forschungsgemeinschaft, DFG).

APPENDIX A: SPIN WAVE DISPERSIONS

In the magnetic Brillouin zone, where $\sum_{\mathbf{q}} = N/2$, there are two spin wave branches, with dispersions given by [23]

$$\omega_{\pm}(\mathbf{q}) = 4J_{\mathrm{av}}S\sqrt{(1\mp B_{\mathbf{q}})^2 + A_{\mathbf{q}}^2}. \tag{A1}$$

In this expression, $S = 1/2$, $J_{\mathrm{av}} = J + (\Gamma_{\parallel} + \Gamma_{\perp})/2$,

$$\begin{aligned} A_{\mathbf{q}} &= \frac{1}{4J_{\mathrm{av}}}[J_1\cos(q_x a) + J_2\cos(q_y a)], \\ B_{\mathbf{q}} &= -\frac{1}{4J_{\mathrm{av}}}[J_3\cos(q_x a) + J_4\cos(q_y a)], \end{aligned} \tag{A2}$$

and

$$\begin{aligned} J_1 &= 2J + \Gamma_{zz} + \Gamma_{\parallel}\sin^2\phi + \Gamma_{\perp}\cos^2\phi, \\ J_2 &= 2J + \Gamma_{zz} + \Gamma_{\parallel}\cos^2\phi + \Gamma_{\perp}\sin^2\phi, \\ J_3 &= -\Gamma_{zz} + \Gamma_{\parallel}\sin^2\phi + \Gamma_{\perp}\cos^2\phi, \\ J_4 &= -\Gamma_{zz} + \Gamma_{\parallel}\cos^2\phi + \Gamma_{\perp}\sin^2\phi. \end{aligned} \tag{A3}$$

These can be rewritten in terms of the coupling constants $\bar{J}$ and $\bar{\Gamma}_{\parallel}$ entering the Hamiltonian terms in Eq. (5) by making the replacements $J = \bar{J} + (1/3)\bar{\Gamma}_{\parallel}$, $\Gamma_{\parallel} = (2/3)\bar{\Gamma}_{\parallel}$, and $\Gamma_{\perp} = \Gamma_{zz} = -(1/3)\bar{\Gamma}_{\parallel}$.

APPENDIX B: ENERGY MINIMIZATION FOR A BILAYER

The ground-state magnetic energy of the layered system can be written as a sum over bilayer contributions (per spin and per layer):

$$\begin{aligned} E(\phi_1,\phi_2) &= -\frac{K}{2}[\cos(4\phi_1) + \cos(4\phi_2)] \\ &\quad - B\cos[2(\phi_1 - \phi_2)] - A\sin(\phi_1 + \phi_2) \\ &= -K\cos(2\phi_+)\cos(2\phi_-) - B\cos(2\phi_-) \\ &\quad - A\sin\phi_+, \end{aligned}$$

where the angles ϕ_1 and ϕ_2 define orientations (say, with respect to the x axis) in two adjacent planes and $\phi_{\pm} = \phi_1 \pm \phi_2$. We note that both K and B are positive. In the subsequent discussion, the coupling A is chosen positive as well by taking into account the fact that for $A < 0$ the simultaneous change of signs, $\phi_1 \to -\phi_1$ and $\phi_2 \to -\phi_2$, retains the expression for $E(\phi_1,\phi_2)$ invariant.

Minimizing $E(\phi_1,\phi_2)$ we find four possible extrema solutions for ϕ_1 and ϕ_2 and the respective energies (n and m are integers):

$$\phi_-^{(1)} = m\pi, \qquad \phi_+^{(1)} = \frac{\pi}{2} + 2n\pi, \qquad E^{(1)} = K - B - A, \tag{B1}$$

which is possible if $B > K$;

$$\begin{aligned} &\phi_-^{(2)} = m\pi, \quad \phi_+^{(2)} = \arcsin\frac{A}{4K} + 2n\pi, \\ &E^{(2)} = -K - B - \frac{A^2}{8K}, \end{aligned} \tag{B2}$$

with the requirement $A < 4K$;

$$\begin{aligned} &\phi_-^{(3)} = (2m+1)\frac{\pi}{2}, \qquad \phi_+^{(3)} = \frac{\pi}{2} + 2n\pi, \\ &E^{(3)} = B - K - A, \end{aligned} \tag{B3}$$

which is possible if $B < K$;

$$\begin{aligned} \sin\phi_+^{(4)} &= \sqrt{\frac{1 + B/K}{2}}, \\ \cos(2\phi_-^{(4)}) &= \frac{A}{4K}\sqrt{\frac{2}{1 + B/K}}, \\ E^{(4)} &= -A\sqrt{\frac{1 + B/K}{2}}, \end{aligned} \tag{B4}$$

which may occur in the parameter region $B < K$, $A < K\sqrt{\frac{1+B/K}{2}}$.

Comparison of the energies of the four possible ground-state configurations shows that three of them, Eqs. (B1)–(B3), occur in different domains of the A-B parameter space. In the region $B > K$ and $A > 4K$, the most stable is the configuration (B1) with $\phi_1^{(1)} = (\pi/4) + n(\pi/2)$ and $\phi_2^{(1)} = \phi_1^{(1)} - m\pi$, which means that the spins (staggered magnetizations) are along one of the $\langle 110\rangle$ axes and in two adjacent planes the spin alignment is either collinear or anticollinear. Next, in the region with $B > K$, $0 < A < 4K$, the second configuration (B2) with $\phi_1^{(2)} = \frac{1}{2}\arcsin(A/4K) + n(\pi/2)$ and $\phi_2^{(1)} = \phi_1^{(1)} - m\pi$ is realized. Here, the collinear-anticollinear alignment in successive layers still persists. However, the preferred direction is specified by $A/4K$. In the region with $B < K$, $A > 4K$, the third configuration (B3) with $\phi_1^{(3)} = m(\pi/2)$ and $\phi_2^{(3)} = \phi_1^{(3)} - (\pi/2) - m\pi$ is the most stable, which corresponds to having the magnetization along one of the $\langle 100\rangle$ axes with two directions in successive layers being rotated by 90°. Finally, for $B < K$ and $A < 4K$, the fourth solution (B4) has the highest energy and two of the other configurations, i.e., Eqs. (B2) and (B3), compete to give the phase boundary depicted in Fig. 2.

Ising degrees of freedom.—It is clear that the above classical minima of a Ba214 bilayer are also the minima of the infinite system. In all phases, however, there is still an Ising degree of freedom per layer, which is not fixed by the couplings considered here. In phase I, for example, we may flip the directions of all spins in any plane, since the energy is the same for both collinear and anticollinear relative orientations between adjacent planes. The eventual removal of this remaining macroscopic Ising degree of freedom must originate from higher-order processes or farther-neighbor couplings [22].

[1] J. G. Bednorz and K. A. Müller, *Possible High-T_c Superconductivity in the Ba-La-Cu-O System*, Z. Phys. B **64**, 189 (1986).

[2] Y. Kamihara, T. Watanabe, M. Hirano, and H. Hosono, *Iron-Based Layered Superconductor* $La[O_{1-x}F_x]FeAs$ *($x = 0.05$–0.12) with* $T_c = 26$ K, J. Am. Chem. Soc. **130**, 3296 (2008).

[3] P. A. Lee, N. Nagaosa, and X.-G. Wen, *Doping a Mott Insulator: Physics of High-Temperature Superconductivity*, Rev. Mod. Phys. **78**, 17 (2006).

[4] D. J. Singh and M.-H. Du, *Density Functional Study of* $LaFeAsO_{1-x}F_x$*: A Low Carrier Density Superconductor Near Itinerant Magnetism*, Phys. Rev. Lett. **100**, 237003 (2008); T. Yildirim, *Frustrated Magnetic Interactions, Giant Magnetoelastic Coupling, and Magnetic Phonons in Iron Pnictides*, Physica (Amsterdam) **469C**, 425 (2009).

[5] B. Keimer, A. Aharony, A. Auerbach, R. J. Birgeneau, A. Cassanho, Y. Endoh, R. W. Erwin, M. A. Kastner, and G. Shirane, *Néel Transition and Sublattice Magnetization of Pure and Doped* La_2CuO_4, Phys. Rev. B **45**, 7430 (1992).

[6] D. Vaknin, S. K. Sinha, C. Stassis, L. L. Miller, and D. C. Johnston, *Antiferromagnetism in* $Sr_2CuO_2Cl_2$, Phys. Rev. B **41**, 1926 (1990).

[7] M. Greven, R. J. Birgeneau, Y. Endoh, M. A. Kastner, M. Matsuda, and G. Shirane, *Neutron Scattering Study of the Two-Dimensional Spin* $S = 1/2$ *Square-Lattice Heisenberg Antiferromagnet* $Sr_2CuO_2Cl_2$, Z. Phys. B **96**, 465 (1995).

[8] B. J. Kim, H. Ohsumi, T. Komesu, S. Sakai, T. Morita, H. Takagi, and T. Arima, *Phase-Sensitive Observation of a Spin-Orbital Mott State in* Sr_2IrO_4, Science **323**, 1329 (2009).

[9] B. J. Kim, H. Jin, S. J. Moon, J.-Y. Kim, B.-G. Park, C. S. Leem, J. Yu, T. W. Noh, C. Kim, S.-J. Oh, J.-H. Park, V. Durairaj, G. Cao, and E. Rotenberg, *Novel* $J = 1/2$ *Mott State Induced by Relativistic Spin-Orbit Coupling in* Sr_2IrO_4, Phys. Rev. Lett. **101**, 076402 (2008).

[10] G. Jackeli and G. Khaliullin, *Mott Insulators in the Strong Spin-Orbit Coupling Limit: From Heisenberg to a Quantum Compass and Kitaev Models*, Phys. Rev. Lett. **102**, 017205 (2009).

[11] J. Kim, D. Casa, M. H. Upton, T. Gog, Y.-J. Kim, J. F. Mitchell, M. van Veenendaal, M. Daghofer, J. van den Brink, G. Khaliullin, and B. J. Kim, *Magnetic Excitation Spectra of* Sr_2IrO_4 *Probed by Resonant Inelastic X-Ray Scattering: Establishing Links to Cuprate Superconductors*, Phys. Rev. Lett. **108**, 177003 (2012).

[12] S. Boseggia, R. Springell, H. C. Walker, H. M. Rønnow, C. Rüegg, H. Okabe, M. Isobe, R. S. Perry, S. P. Collins, and D. F. McMorrow, *Robustness of Basal-Plane Antiferromagnetic Order and the* $J_{\mathrm{eff}}=1/2$ *State in Single-Layer Iridate Spin-Orbit Mott Insulators*, Phys. Rev. Lett. **110**, 117207 (2013).

[13] S. K. Choi, R. Coldea, A. N. Kolmogorov, T. Lancaster, I. I. Mazin, S. J. Blundell, P. G. Radaelli, Y. Singh, P. Gegenwart, K. R. Choi, S.-W. Cheong, P. J. Baker, C. Stock, and J. Taylor, *Spin Waves and Revised Crystal Structure of Honeycomb Iridate* Na_2IrO_3, Phys. Rev. Lett. **108**, 127204 (2012).

[14] J. H. M. Thornley, *The Magnetic Properties of* $(IrX_6)^{2-}$ *Complexes*, J. Phys. C **1**, 1024 (1968).

[15] B. H. Kim, G. Khaliullin, and B. I. Min, *Magnetic Couplings, Optical Spectra, and Spin-Orbit Exciton in* $5d$ *Electron Mott Insulator* Sr_2IrO_4, Phys. Rev. Lett. **109**, 167205 (2012).

[16] N. B. Perkins, Y. Sizyuk, and P. Wölfle, *Interplay of Many-Body and Single-Particle Interactions in Iridates and Rhodates*, Phys. Rev. B **89**, 035143 (2014).

[17] J. Chaloupka, G. Jackeli, and G. Khaliullin, *Zigzag Magnetic Order in the Iridium Oxide* Na_2IrO_3, Phys. Rev. Lett. **110**, 097204 (2013).

[18] K. Foyevtsova, H. O. Jeschke, I. I. Mazin, D. I. Khomskii, and R. Valentí, *Ab Initio Analysis of the Tight-Binding Parameters and Magnetic Interactions in* Na_2IrO_3, Phys. Rev. B **88**, 035107 (2013).

[19] V. M. Katukuri, S. Nishimoto, V. Yushankhai, A. Stoyanova, H. Kandpal, S. K. Choi, R. Coldea, I. Rousochatzakis, L. Hozoi, and J. van den Brink, *Kitaev Interactions between* $j = 1/2$ *Moments in Honeycomb* Na_2IrO_3 *Are Large and Ferromagnetic: Insights from Ab Initio Quantum Chemistry Calculations*, New J. Phys. **16**, 013056 (2014).

[20] H. Gretarsson, J. P. Clancy, Y. Singh, P. Gegenwart, J. P. Hill, J. Kim, M. H. Upton, A. H. Said, D. Casa, T. Gog, and Y.-J. Kim, *Magnetic Excitation Spectrum of* Na_2IrO_3 *Probed with Resonant Inelastic X-Ray Scattering*, Phys. Rev. B **87**, 220407 (2013).

[21] P. W. Anderson, *Antiferromagnetism. Theory of Superexchange Interaction*, Phys. Rev. **79**, 350 (1950); J. Kanamori, *Theory of the Magnetic Properties of Ferrous and Cobaltous Oxides, I*, Prog. Theor. Phys. **17**, 177 (1957); *Theory of the Magnetic Properties of Ferrous and Cobaltous OxidesII* **17**, 197 (1957); J. B. Goodenough, *An Interpretation of the Magnetic Properties of the Perovskite-Type Mixed Crystals* $La_{1-x}Sr_xCoO_{3-\lambda}$, J. Phys. Chem. Solids **6**, 287 (1958); J. Kanamori, *Superexchange Interaction and Symmetry Properties of Electron Orbitals*, J. Phys. Chem. Solids **10**, 87 (1959).

[22] T. Yildirim, A. B. Harris, and E. F. Shender, *Three-Dimensional Ordering in bct Antiferromagnets due to Quantum Disorder*, Phys. Rev. B **53**, 6455 (1996).

[23] A. Aharony, O. Entin-Wohlman, and A. B. Harris, *Dynamical Properties of Unconventional Magnetic Systems* (Kluwer Academic, Dordrecht, 1998).

[24] C. Martins, M. Aichhorn, L. Vaugier, and S. Biermann, *Reduced Effective Spin-Orbital Degeneracy and*

Spin-Orbital Ordering in Paramagnetic Transition-Metal Oxides: Sr_2IrO_4 *versus* Sr_2RhO_4, Phys. Rev. Lett. **107**, 266404 (2011).

[25] R. Arita, J. Kuneš, A. V. Kozhevnikov, A. G. Eguiluz, and M. Imada, *Ab Initio Studies on the Interplay between Spin-Orbit Interaction and Coulomb Correlation in* Sr_2IrO_4 *and* Ba_2IrO_4, Phys. Rev. Lett. **108**, 086403 (2012).

[26] K. I. Kugel and D. I. Khomskii, *Crystal Structure and Magnetic Properties of Substances with Orbital Degeneracy*, Sov. Phys. JETP **37**, 725 (1973).

[27] M. Moretti-Sala, M. Rossi, S. Boseggia, J. Akimitsu, N. B. Brookes, M. Isobe, M. Minola, H. Okabe, H. M. Rønnow, L. Simonelli, D. F. McMorrow, and G. Monaco, *Orbital Occupancies and the Putative* $j_{\mathrm{eff}} = 1/2$ *Ground State in* Ba_2IrO_4*: A Combined Oxygen K Edge XAS and RIXS Study*, Phys. Rev. B **89**, 121101(R) (2014).

[28] H. Okabe, M. Isobe, E. Takayama-Muromachi, A. Koda, S. Takeshita, M. Hiraishi, M. Miyazaki, R. Kadono, Y. Miyake, and J. Akimitsu, Ba_2IrO_4*: A Spin-Orbit Mott Insulating Quasi-Two-Dimensional Antiferromagnet*, Phys. Rev. B **83**, 155118 (2011).

[29] T. Helgaker, P. Jørgensen, and J. Olsen, *Molecular Electronic-Structure Theory* (Wiley, Chichester, England, 2000).

[30] C. de Graaf, C. Sousa, and R. Broer, *Ionization and Excitation Energies in CuCl and NiO within Different embedding Schemes*, J. Mol. Struct. Theochem **458**, 53 (1998).

[31] L. Hozoi, L. Siurakshina, P. Fulde, and J. van den Brink, *Ab Initio Determination of Cu* 3*d Orbital Energies in Layered Copper Oxides*, Sci. Rep. **1**, 65 (2011).

[32] L. Hozoi and M. Laad, *Quasiparticle Bands in Cuprates by Quantum-Chemical Methods: Towards an Ab Initio Description of Strong Electron Correlations*, Phys. Rev. Lett. **99**, 256404 (2007).

[33] V. M. Katukuri, H. Stoll, J. van den Brink, and L. Hozoi, *Ab initio Determination of Excitation Energies and Magnetic Couplings in Correlated Quasi-Two-Dimensional Iridates*, Phys. Rev. B **85**, 220402 (2012).

[34] N. A. Bogdanov, V. M. Katukuri, H. Stoll, J. van den Brink, and L. Hozoi, *Post-Perovskite* $CaIrO_3$*: A* $j = 1/2$ *Quasi-One-Dimensional Antiferromagnet*, Phys. Rev. B **85**, 235147 (2012); M. Moretti-Sala, K. Ohgushi, A. Al-Zein, Y. Hirata, G. Monaco, and M. Krisch, $CaIrO_3$*: A Spin-Orbit Mott Insulator beyond the* $j = 1/2$ *Ground State*, Phys. Rev. Lett. **112**, 176402 (2014).

[35] N. A. Bogdanov, R. Maurice, I. Rousochatzakis, J. van den Brink, and L. Hozoi, *Magnetic State of Pyrochlore* $Cd_2Os_2O_7$ *Emerging from Strong Competition of Ligand Distortions and Longer-Range Crystalline Anisotropy*, Phys. Rev. Lett. **110**, 127206 (2013).

[36] L. Hozoi, A. H. de Vries, A. B. van Oosten, R. Broer, J. Cabrero, and C. de Graaf, *Theoretical Characterization of the Ground and Optically Excited States of* α'-$Na_2V_2O_5$, Phys. Rev. Lett. **89**, 076407 (2002).

[37] R. Maurice, P. Verma, J. M. Zadrozny, S. Luo, J. Borycz, J. R. Long, D. G. Truhlar, and L. Gagliardi, *Single-Ion Magnetic Anisotropy and Isotropic Magnetic Couplings in the Metal-Organic Framework Fe2(dobdc)*, Inorg. Chem. **52**, 9379 (2013).

[38] H.-J. Werner, P. J. Knowles, G. Knizia, F. R. Manby, and M. Schütz, MOLPRO 2012, http://www.molpro.net.

[39] D. Figgen, K. A. Peterson, M. Dolg, and H. Stoll, *Energy-Consistent Pseudopotentials and Correlation Consistent Basis Sets for the* 5*d Elements Hf–Pt*, J. Chem. Phys. **130**, 164108 (2009).

[40] P. Fuentealba, L. von Szentpaly, H. Preuss, and H. Stoll, *Pseudopotential Calculations for Alkaline-Earth Atoms*, J. Phys. B **18**, 1287 (1985).

[41] T. H. Dunning, *Gaussian Basis Sets for Use in Correlated Molecular Calculations. I. The Atoms Boron through Neon and Hydrogen*, J. Chem. Phys. **90**, 1007 (1989).

[42] K. Pierloot, B. Dumez, P.-O. Widmark, and B. Roos, *Density Matrix Averaged Atomic Natural Orbital (ANO) Basis Sets for Correlated Molecular Wave Functions*, Theor. Chim. Acta **90**, 87 (1995).

[43] K. Fink, R. Fink, and V. Staemmler, *Ab Initio Calculation of the Magnetic Exchange Coupling in Linear Oxo-Bridged Binuclear Complexes of Titanium(III), Vanadium(III), and Chromium(III)*, Inorg. Chem. **33**, 6219 (1994).

[44] A. B. van Oosten, R. Broer, and W. C. Nieuwpoort, *Heisenberg Exchange Enhancement by Orbital Relaxation in Cuprate Compounds*, Chem. Phys. Lett. **257**, 207 (1996).

[45] R. Broer, L. Hozoi, and W. C. Nieuwpoort, *Nonorthogonal Approaches to the Study of Magnetic Interactions*, Mol. Phys. **101**, 233 (2003).

[46] C. J. Calzado, S. Evangelisti, and D. Maynau, *Local Orbitals for the Truncation of Inactive Space: Application to Magnetic Systems*, J. Phys. Chem. A **107**, 7581 (2003).

[47] A. Berning, M. Schweizer, H.-J. Werner, P. J. Knowles, and P. Palmieri, *Spin-Orbit Matrix Elements for Internally Contracted Multireference Configuration Interaction Wave Functions*, Mol. Phys. **98**, 1823 (2000).

[48] The higher-lying spin-orbit states imply an excitation energy of at least 0.6 eV. This gap concerns the $j = 1/2$ to $j = 3/2$ transitions [11,53].

[49] The energies of those two states differ by not more than 0.1 cm^{-1} in the spin-orbit ROHF, CASSCF, and MRCI calculations.

[50] Y. J. Guo, J.-M. Langlois, and W. A. Goddard, *Electronic Structure and Valence-Bond Band Structure of Cuprate Superconducting Materials*, Science **239**, 896 (1988).

[51] R. L. Martin and P. W. Saxe, *Ab Initio Electronic Structure Theory for a Cluster Model of* $La_{2-x}Sr_xCuO_4$, Int. J. Quantum Chem. **34**, 237 (1988).

[52] D. Muñoz, F. Illas, and I. de P. R. Moreira, *Accurate Prediction of Large Antiferromagnetic Interactions in High-*T_c $HgBa_2Ca_{n-1}Cu_nO_{2n+2+\delta}$ ($n = 2, 3$) *Superconductor Parent Compounds*, Phys. Rev. Lett. **84**, 1579 (2000).

[53] V. M. Katukuri, K. Roszeitis, V. Yushankhai, A. Mitrushchenkov, H. Stoll, M. van Veenendaal, P. Fulde, J. van den Brink, and L. Hozoi, *Electronic Structure of Low-Dimensional* $4d^5$ *Oxides: Interplay of Ligand Distortions, Overall Lattice Anisotropy, and Spin-Orbit Interactions*, Inorg. Chem. **53**, 4833 (2014).

[54] R. Dingle, *The Near Infrared Absorption Spectrum of Tris Acetylacetonato Osmium (III)*, J. Mol. Spectrosc. **18**, 276 (1965).

[55] G. C. Allen, R. Al-Mobarak, G. A. M. El-Sharkawi, and K. D. Warren, *Electronic Spectra of the Hexahalo Anions of Osmium(IV) and Iridium(IV)*, Inorg. Chem. **11**, 787 (1972).

[56] B. Andlauer, J. Schneider, and W. Tolksdorf, *Optical Absorption, Fluorescence, and Electron Spin Resonance*

of Ir^{4+} *on Octahedral Sites in* $Y_3Ga_5O_{12}$, Phys. Status Solidi B **73**, 533 (1976).

[57] S. Ping, H. Lv, and Z. Wen-Chen, *Theoretical Studies of the Spin-Hamiltonian Parameters and Their Stress Dependences for* Ru^{3+} *and* Ir^{4+} *Ions in* $Y_3Ga_5O_{12}$ *Crystals*, J. Alloys Compd. **474**, 31 (2009).

[58] Z. Nussinov and E. Fradkin, *Discrete Sliding Symmetries, Dualities, and Self-Dualities of Quantum Orbital compass Models and* $p+ip$ *Superconducting arrays*, Phys. Rev. B **71**, 195120 (2005).

[59] F. Trousselet, A. M. Oleś, and P. Horsch, *Magnetic Properties of Nanoscale Compass-Heisenberg Planar Clusters*, Phys. Rev. B **86**, 134412 (2012).

[60] A. Mishra, M. Ma, F.-C. Zhang, S. Guertler, L.-H. Tang, and S. Wan, *Directional Ordering of Fluctuations in a Two-Dimensional Compass Model*, Phys. Rev. Lett. **93**, 207201 (2004).

[61] Z. Nussinov, M. Biskup, L. Chayes, and J. van den Brink, *Orbital Order in Classical Models of Transition-Metal Compounds*, Europhys. Lett. **67**, 990 (2004).

[62] S. Wenzel, W. Janke, and A. M. Läuchli, *Reexamining the Directional-Ordering Transition in the Compass Model with Screw-Periodic Boundary Conditions*, Phys. Rev. E **81**, 066702 (2010).

[63] G. Khaliullin, *Order from Disorder: Quantum Spin Gap in Magnon Spectra of* $LaTiO_3$, Phys. Rev. B **64**, 212405 (2001).

[64] J. Dorier, F. Becca, and F. Mila, *Quantum Compass Model on the Square Lattice*, Phys. Rev. B **72**, 024448 (2005).

[65] D. Haskel, G. Fabbris, M. Zhernenkov, P. P. Kong, C. Q. Jin, G. Cao, and M. van Veenendaal, *Pressure Tuning of the Spin-Orbit Coupled Ground State in* Sr_2IrO_4, Phys. Rev. Lett. **109**, 027204 (2012).

[66] A. Lupascu, J. P. Clancy, H. Gretarsson, Z. Nie, J. Nichols, J. Terzic, G. Cao, S. S. A. Seo, Z. Islam, M. H. Upton, J. Kim, D. Casa, T. Gog, A. H. Said, V. M. Katukuri, H. Stoll, L. Hozoi, J. van den Brink, and Y.-J. Kim, *Tuning Magnetic Coupling in* Sr_2IrO_4 *Thin Films with Epitaxial Strain*, Phys. Rev. Lett. **112**, 147201 (2014).